PREPARED FOR THE U.S. DEPARTMENT OF ENERGY,
UNDER CONTRACT DE-AC02-76-CHO-3073

PPPL-2745
UC-420,426

PPPL-2745

VISIBLE CHARGE EXCHANGE RECOMBINATION SPECTROSCOPY ON TFTR

BY

B. STRATTON, R.J. FONCK, K.P. JAEHNIG, N. SCHECHTMAN,
E.J. SYNAKOWSKI

March 1991

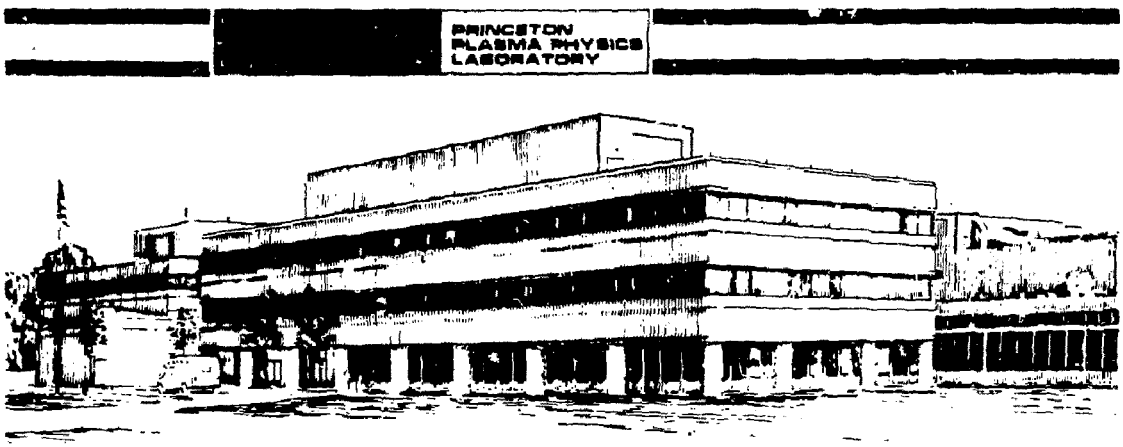

PRINCETON UNIVERSITY, PRINCETON, NEW JERSEY

NOTICE

NOTICE

Available from:

National Technical Information Service
U.S. Department of Commerce
5285 Port Royal Road
Springfield, Virginia 22161
703-487-4650

Use the following price codes when ordering:

Price: Printed Copy A03
Microfiche A01

PPPL--2745

DE91 011105

VISIBLE CHARGE EXCHANGE RECOMBINATION SPECTROSCOPY ON TFTR

B. C. Stratton, R. J. Fonck,* K. P. Jaehnig,** N. Schechtman, E. J. Synakowski
Princeton University, Plasma Physics Laboratory, Princeton, NJ, 08543, USA

ABSTRACT

Visible charge exchange recombination spectroscopy is routinely used to measure the time evolution of the ion temperature (T_i) and toroidal rotation velocity (v_ϕ) profiles on TFTR. These measurements are made with the CHERS diagnostic, a fiber-optically coupled spectrometer equipped with a two-dimensional photodiode array detector which provides both spectral and spatial resolution. The instrumentation, data analysis techniques, and examples of T_i and v_ϕ measurements are described. Recently, CHERS has been used to perform impurity transport experiments: radial profiles of diffusivities and convective velocities for helium and iron have been deduced from measurements of the time evolutions of He^{2+} and Fe^{24+} profiles following impurity injection. Examples of these measurements are given.

*Present address: Department of Nuclear Engineering and Engineering Physics, University of Wisconsin, Madison, WI 53706 USA.
**Present address: Space Astronomy Laboratory, University of Wisconsin, Madison, WI 53706 USA.

To be published in The Proceedings of the IAEA Technical Committee Meeting on Time Resolved Two- and Three-Dimensional Plasma Diagnostics, held in Nagoya, Japan, November 19-22, 1990.

INTRODUCTION

Charge exchange recombination spectroscopy (CXRS) [1] has become a standard technique for measurement of the ion temperature (T_i) and toroidal rotation velocity (v_ϕ) on tokamaks in recent years. Line radiation excited by recombination of an impurity ion (usually fully ionized) with a hydrogen or deuterium atom in a neutral beam is observed, and T_i and v_ϕ are deduced from the Doppler broadening and shift of the line. CXRS has the advantage that the emission is localized to the region of intersection of the beam and spectrometer sightline, making it possible to obtain accurate spatial profiles of T_i and v_ϕ from spatially-resolved observations of a single spectral line. These measurements are usually made in the visible region of the spectrum, which allows fiber optics to be used to couple the spectrometer to the tokamak and therefore makes radiation shielding simple. CXRS has also been used to measure profiles of light impurities [2, 3] and their absolute densities [4, 5], and to study transport of both light [6, 7] and medium-Z [8] impurities.

CXRS in the visible region of the spectrum on TFTR is performed using the CHERS diagnostic [9], a visible and near-UV spectrometer equipped with a two-dimensional detector which provides both spectral and spatial resolution. This paper describes the CHERS instrumentation, data analysis techniques, examples of T_i and v_ϕ measurements, and recent studies of helium and iron ion transport.

INSTRUMENTATION

Figure 1 shows the locations of the heating neutral beams and the diagnostic neutral beam on TFTR. There are four heating beamlines: beamlines 1 and 2 inject in the counter direction relative to the plasma current and beamlines 4 and 5 inject in the co-direction. Each beamline has three ion sources sharing a common neutralization gas cell and produces three independent beams, designated A, B, and C. The heating beams operate in deuterium with energies typically in the 90-110 keV range, and the diagnostic beam operates in hydrogen at 60-70 keV. The spatial coverage of the principal arrays of CHERS sightlines are shown and are labeled with the letter designating the "bay", or region between adjacent toroidal field coils, at which the viewing optics are located. The arrays located at bay K and bay P are routinely used for T_i and v_ϕ measurements. These arrays see the heating beams with tangential views lying in the plasma midplane; the bay K array views the beams injected by beamline 4, while the bay P array sees the beamline 1 beams. Note that the inner sightlines of the bay K array also see the beamline 5 beams and therefore see two regions of the plasma of different temperature when both beamlines 4 and 5 are used; in order to avoid the resulting complications in the analysis,

the bay K array is normally used only when beamline 5 is not in use. The sightlines of the bay K and bay P arrays are close to tangent to the flux surfaces and, as a result, the intersection of a given sightline with each of the three beams produced by a heating beamline occurs in a region of the plasma with approximately the same temperature. Thus, viewing across the three beams injected by one beamline does not result in significant loss of spatial localization of the signal. There are also two arrays viewing the diagnostic beam (not shown in Fig. 1): a tangential one at bay E and a vertical one looking down on the diagnostic beam at bay A.

Each array consists of a group of high-purity quartz fibers with their ends arranged in a row and viewing the plasma through a quartz focusing lens and a window on the vacuum vessel. The windows have shutters that may be closed to prevent coating of the inner surface during discharge cleaning. The bay P array consists of 18 fibers of 0.6 mm diameter, while the other arrays have 12 fibers of 1 mm diameter. The sightlines of the bay K array intersect the beamline 4 beams at major radii (R) of 2.34-3.34 m with 0.1 m separation between channels, and the bay P array views the region R=2.50-3.00 m with 0.05 m channel separation. (The views of the outer six fibers of the bay P array are presently obstructed by structures inside the vacuum vessel; this will be corrected in the near future.) The bay K array therefore provides coverage of the outer half of a standard TFTR plasma with R=2.45 m and a=0.80 m, and the bay P array covers the core region of such a discharge. The spatial resolution of the measurements is determined by the radial extent of the region viewed by each fiber, which is 0.03-0.05 m. One fiber in each array views a mercury lamp used for measurement of the instrumental line shape.

The fibers run to a 0.6 m, f/5.7 Czerny-Turner spectrometer, shown schematically in Fig. 2, which is located in the basement of the TFTR test cell. The images of the output ends of the fibers in each array are directed onto the entrance slit in a vertical row via a galvanometer-driven mirror used to select which fiber array is used at a given time. A remotely adjustable lens is used to focus the images. The useful spectral coverage of the system of 2800-7300 Å is limited at the short wavelength end by a rapid decrease in the transmission of the fibers below 3000 Å. The detector is a two-dimensional image-intensified photodiode array located in the output focal plane of the spectrometer, and, as shown in Fig. 2, it is oriented so that the directions of dispersion and imaging are aligned with the rows and columns of pixels. Each pixel in the 128 × 128 photodiode array (Reticon MC9128) has dimensions of 60 μm × 60 μm. The entire detector is magnetically shielded in order to prevent distortion of the image by stray magnetic fields.

A block diagram of the data acquisition system and electronics is shown in Fig. 3. The data are read out from the detector at 8 Mhz and are digitized at the 10 bit level by an image processor (Recognition Concepts Inc. Trapix 55/64) interfaced to the Q-bus of a DEC

microVAX II computer. The detector analog signal and detector synchronization signals are transmitted by 350 m fiber optic links to the image processor and computer, which are located near the TFTR control room. An ethernet link connects the microVAX to the laboratory's VAX cluster, where the data are permanently archived, and to a VAXstation 3100 workstation dedicated to automatic analysis of the data following a discharge. Up to 64 time points during the discharge may be acquired, resulting in 2 megabytes of raw data per shot. The detector timing and other functions, such as fiber bank selection, detector high voltage, the spectrometer wavelength drive, and window shutter control, are controlled through through CAMAC interfaces connected to the microVAX by a fiber-optic CAMAC serial highway.

ION TEMPERATURE AND ROTATION VELOCITY MEASUREMENTS

The C^{5+} 5292 Å line (n=7-8) is usually used for T_i and v_ϕ measurements because it is strong and unblended. Figure 4 shows measurements of this line from edge and central channels in the bay K array taken in a supershot discharge produced by injecting 21 MW of beam power into a low density deuterium plasma at 1.3 MA plasma current. The total power in the beamline 4 beams was 7.1 MW at an average energy of 99 keV. The spectra are from a single frame, or readout of the detector, of 0.02 s integration time and are fit using a nonlinear least-squares-fitting routine with a single Gaussian plus a linear background convolved with the measured instrumental function. For bay K, the measured instrumental width at 5292 Å is 6 Å, which is equivalent to T_i=2.6 keV. A "dark frame" of data taken approximately 15 s after the end of the discharge, when the detector is not exposed to light, is subtracted from the data to remove the detector dark current, and a white-field calibration is applied to correct for pixel-to-pixel variations in the detector sensitivity. A correction for a measured nonlinearity in the detector gain is also made. The measured dispersion of the spectrometer is used to obtain T_i and v_ϕ from the fitted line width and peak position. The zero velocity reference for the v_ϕ measurement is obtained from the rest position of the line peak measured either prior to beam injection or at the plasma edge where v_ϕ is close to zero.

A frame of data taken immediately after the end of beam injection was subtracted from the spectra shown in Fig. 4 in order to remove the contribution of edge light to the signal. (Edge light on TFTR is emitted with a characteristic temperature of 0.5-2 keV and is excited by electron impact at the plasma edge and possibly charge exchange with thermal neutrals.) This technique works well provided that the intensity of the edge light does not change significantly between the time of interest and the end of the beam pulse; when there is a significant change, a better approach is to fit the total signal with two Gaussians, one for the beam-excited component of the line and the other for the edge

signal. The beamline 5 beams were injected in this discharge but were turned off for 0.05 s around the time of the data shown in Fig. 4, so there is not a second beam-excited component of the line emitted from a lower temperature region of the plasma. In cases when beamline 5 remains on, the data can be fit with two Gaussians, one for each of the beam-excited components of the line; however, this technique can be unreliable, so it is preferable to use the bay P view of the beamline 1 beams in this situation.

Figure 5 shows the T_i and v_ϕ profiles obtained from these data; the error bars include both statistical and systematic errors. The data were analyzed by on the workstation by a DEC command language program which is automatically started when data aquisition is complete. This program runs the line fitting code according to a template which may be edited by the user to change parameters such as the range of time points to be analyzed and the background frame to be subtracted. The results are written into files which can be read by codes such as SNAP, an equilibrium power balance code used to deduce the energy confinement time, as well as ion and electron thermal diffusivities (for examples, see reference 10). This approach has proven quite successful in providing prompt analysis of the data after a shot: T_i and v_ϕ profiles at a single time point, such as those shown in Fig. 5, typically require one and one half minutes of CPU time on the workstation, and the analysis is complete within five minutes of the discharge. A number of experiments have been performed in which the response of the T_i and v_ϕ profiles to a perturbation, for example, a rapid change in beam power or a change in the torque applied to the plasma by the beams, is used to provide information on transport parameters such as ion thermal and momentum diffusivities. These experiments require measurements of the time evolution of the T_i and v_ϕ profiles. Because such analyses are time consuming, they are usually performed as batch jobs on the workstation or VAX cluster.

IMPURITY TRANSPORT MEASUREMENTS

In addition to the measurement of T_i and v_ϕ, CHERS may also be used to accurately measure the radial profiles of impurity ion densities as a function of time. Recent experiments on TFTR have demonstrated that the radial profiles of transport parameters for helium [7] and iron [8] can be deduced from such measurements following impurity injection. Data for both elements were obtained in identical L-mode deuterium discharges with I_p=1.4 MA. The three beamline 4 beams at a total power of 6.7 MW and 100 keV energy were injected for 1.0 s, starting 3.5 s into the discharge. (As a result of the unbalanced beam injection, these plasmas had significant rotation in the co-direction.)

A small helium puff was introduced at 4.2 s and the He^+ 4686 Å line (n=3-4) was observed with the bay K array. The contribution to the total line intensity of emission

from "plume" ions, He^+ ions created by charge exchange of beam neutrals with He^{2+} ions which then drift into the CHERS field-of-view and are excited by electron impact, was calculated and subtracted from the observed intensities to yield the signal due to prompt charge exchange. Profiles of the He^{2+} density as a function of time were obtained from these line intensities, cascade-corrected excitation rates, and beam neutral densities calculated using a beam attenuation code based on the mean free paths of Boley, et al. [11]. He^{2+} profiles at several times following the puff are shown in Fig. 6, along with profiles calculated by the MIST impurity transport code [12] assuming a hollow diffusivity, shown in Fig. 7, and a convective velocity which reproduces the equilibrium He^{2+} profiles; agreement is quite good. As seen in Fig. 6, it is not possible to fit the measured profiles with a spatially constant diffusivity.

For the iron transport measurement, iron was injected at 4.06 s using the laser-blowoff technique, and CHERS was used to observe the Fe^{23+} 5001 Å and Fe^{22+} 5445 Å lines (n=18-19 transitions). Modeling of the line intensities to obtain the time evolutions of the Fe^{24+} and Fe^{23+} profiles (He- and Li-like iron) is similar to that used for helium, except that a plume calculation is not needed because electron-impact excitation of the iron lines is negligible. Time evolutions of the Fe^{24+} densities at four radial locations are shown in Fig. 8, along with values calculated by MIST assuming the moderately hollow diffusivity shown in Fig. 7 plus the neoclassical flux calculated in the Pfirsch-Schlüter regime. Again, agreement is good. Agreement between the measured and calculated Fe^{24+} radial profiles is also good, although the profiles provide less of a constraint on the transport model for iron than for helium due to uncertainties in the dielectronic recombination rates used in MIST.

As seen in Fig. 7, there is a significant difference between iron and helium transport in these discharges. This difference would be difficult to observe using traditional spectroscopic measurements of impurity transport in which the data are modeled by a spatially-constant diffusivity and parametrized convective velocity. Modeling is underway to determine whether or not this difference can be explained by theories of fluctuation-driven transport. Data have also been obtained which will allow comparison of helium, iron, and electron transport in L-mode and supershot plasmas with balanced beam injection.

SUMMARY

The CHERS diagnostic is routinely used to make time resolved measurements of T_i and v_ϕ profiles in TFTR. Aided by recent progress in automating analysis of the data, it is possible to provide T_i and v_ϕ profiles for a wide variety of steady-state and perturbative experiments designed to study ion thermal and momentum transport. In addition,

measurements of radial profiles of transport parameters for helium and iron ions using CHERS demonstrate that this is a powerful technique for the study of particle transport in tokamaks.

ACKNOWLEDGMENTS

The authors would like to thank the entire TFTR group for their support of these measurements and to acknowledge the continuing support of K. M. Young. This work is supported by U. S. Department of Energy Contract No. DE-AC02-76-CHO-3073.

REFERENCES

[1] Fonck, R. J., Darrow, D. S., Jaehnig, K. P., Phys. Rev. A **29** (1984) 3288.

[2] Ida, K., Fonck, R. J., Sesnic, S., Hulse, R. A., LeBlanc, B., Paul, S. F., Nucl. Fusion **29** (1989) 231.

[3] Synakowski, E. J., Bengtson, R. D., Ouroua, A. Wootton, A. J., Kim, S. K., Nucl. Fusion **29** (1989) 311.

[4] Boileau, A., Hellermann, M. von, Horton, L. D., Spence, J., Summers, H. P., Plasma Phys. Controll. Fusion **31** (1989) 571.

[5] Stratton, B. C., Fonck, R. J., Ramsey, A. T., et al., Nucl. Fusion **30** (1990) 675.

[6] Fonck, R. J., Hulse, R. A., Phys. Rev. Lett. **52** (1984) 530.

[7] Synakowski, E. J., Stratton, B. C., Efthimion, P. C., et al., Phys. Rev. Lett. **65** (1990) 2255.

[8] Stratton, B. C., Synakowski, E. J., Efthimion, P. C., et al., Nucl. Fusion, accepted for publication (September 1990).

[9] Jaehnig , K. P., Fonck, R. J., Kindsfather, R. R., Levinton, F. M., Bull. Am. Phys. Soc. **31** (1986) 1612.

[10] Fonck, R. J., Howell, R., Jaehnig, K., et al., Phys. Rev. Lett. **63** (1989) 520.

[11] Boley, C. D., Janev, R. K., Post, D. E., Phys. Rev. Lett. **52** (1984) 534.

[12] Hulse, R. A., Nucl. Technol./Fusion **3** (1983) 447.

FIGURE CAPTIONS

FIG. 1. Locations of TFTR heating neutral beams and diagnostic neutral beam. The regions viewed by the CHERS Bay K and Bay P arrays are shown.

FIG. 2. Schematic diagram of CHERS spectrometer showing coupling of fibers to entrance slit.

FIG. 3. Schematic diagram of CHERS electronics and data acquisition system.

FIG. 4. C^{5+} 5292 Å spectra and fits at the edge (a) and center (b) of a TFTR supershot. The Bay K array viewing the beamline 4 beams and a detector integration time of 0.02 s were used.

FIG. 5. T_i and v_ϕ profiles from the supershot of Fig. 4.

FIG. 6. (a) Helium profiles measured using CHERS at several times following a helium puff. (b) Profiles calculated assuming the diffusivity of Fig. 7 and a convective velocity which reproduces the equilibrium profiles. (c) Profiles calculated assuming a spatially-constant helium diffusivity of 10.0 m^2/s and a convective velocity which reproduces the equilibrium profiles. (d) Same as (c), with a constant diffusivity of 4.0 m^2/s. Closed circles: 0.005 s after puff, open circles: 0.035 s, closed triangles: 0.065 s, open triangles: 0.095 s, closed squares: 0.125 s.

FIG. 7. Helium and iron diffusivities deduced from CHERS data of Figs. 6 and 8.

FIG. 8. Measured (dots) and calculated (lines) time evolutions of Fe^{24+} densities at four radial locations following iron injection. The values are normalized at the time of peak density.

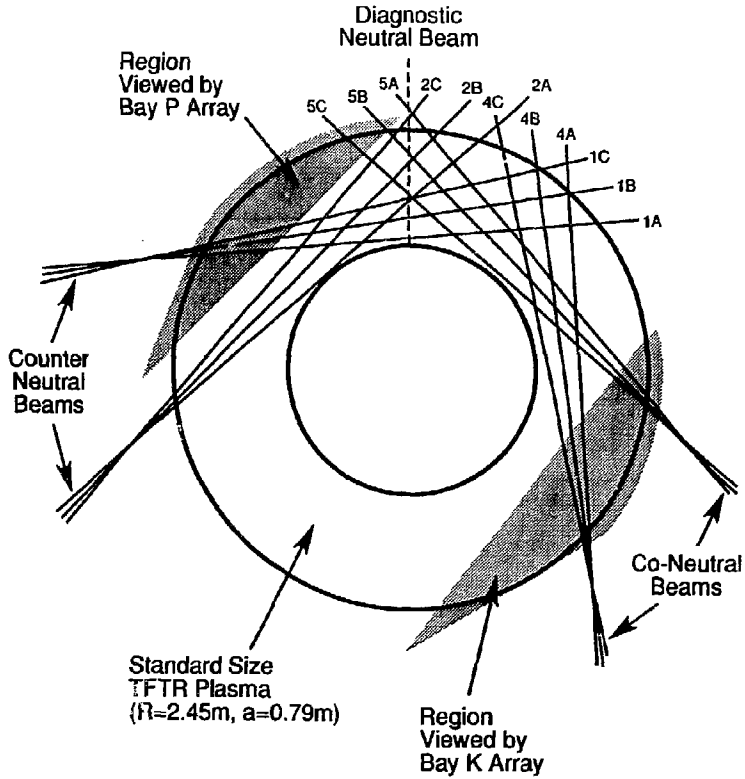
Diagnostic
Neutral Beam
Region
Viewed by
Bay P Array
5C
5B
5A
2C
2B
4C
2A
4B
4A
1C
1B
1A
Counter
Neutral
Beams
Co-Neutral
Beams
Standard Size
TFTR Plasma
(R=2.45m, a=0.79m)
Region
Viewed by
Bay K Array

Fig. 1

TFTR CHERS: Spectrograph Assembly

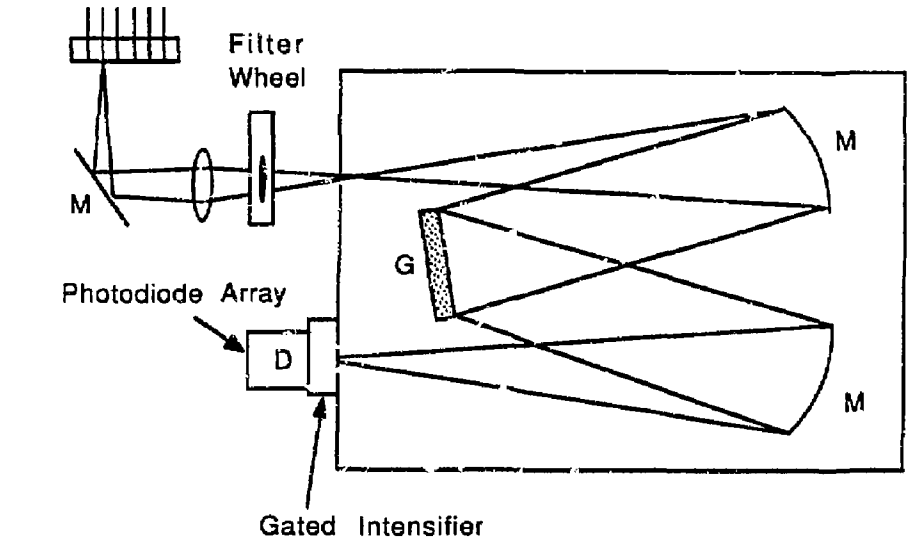

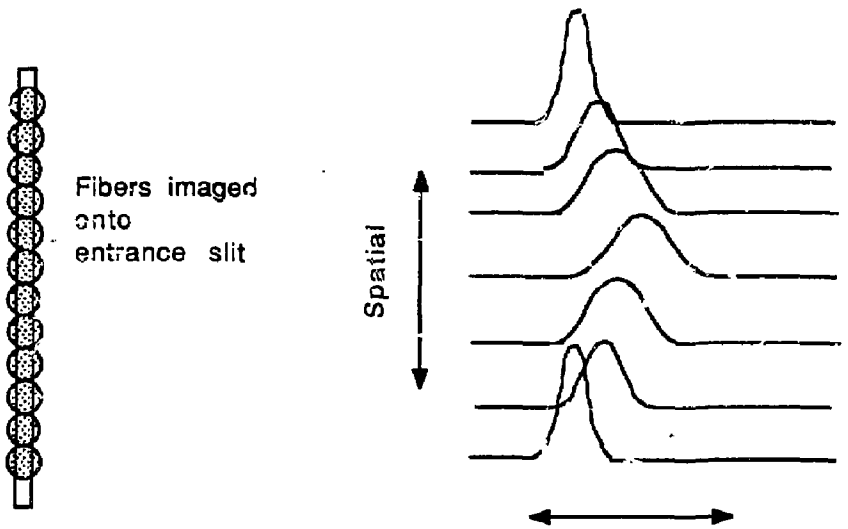

Fig. 2

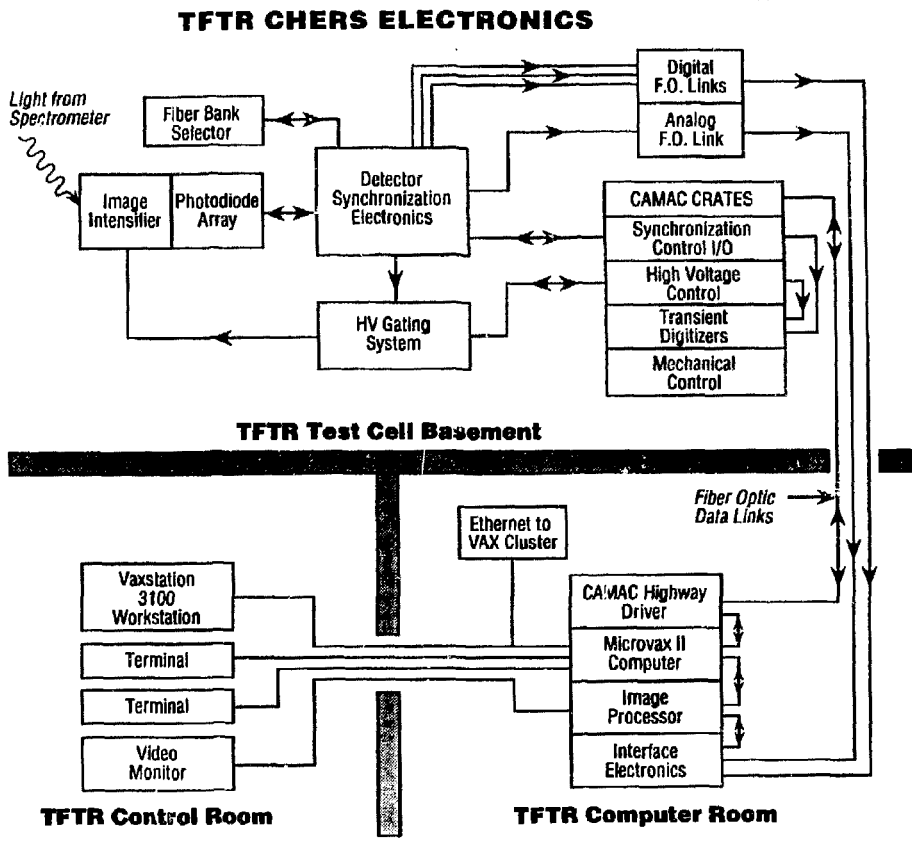
TFTR CHERS ELECTRONICS
Light from Spectrometer
Fiber Bank Selector
Image Intensifier
Photodiode Array
Detector Synchronization Electronics
Digital F.O. Links
Analog F.O. Link
CAMAC CRATES
Synchronization Control I/O
High Voltage Control
Transient Digitizers
Mechanical Control
HV Gating System
TFTR Test Cell Basement
Fiber Optic Data Links
Ethernet to VAX Cluster
Vaxstation 3100 Workstation
Terminal
Terminal
Video Monitor
CAMAC Highway Driver
Microvax II Computer
Image Processor
Interface Electronics
TFTR Control Room
TFTR Computer Room

Fig. 3

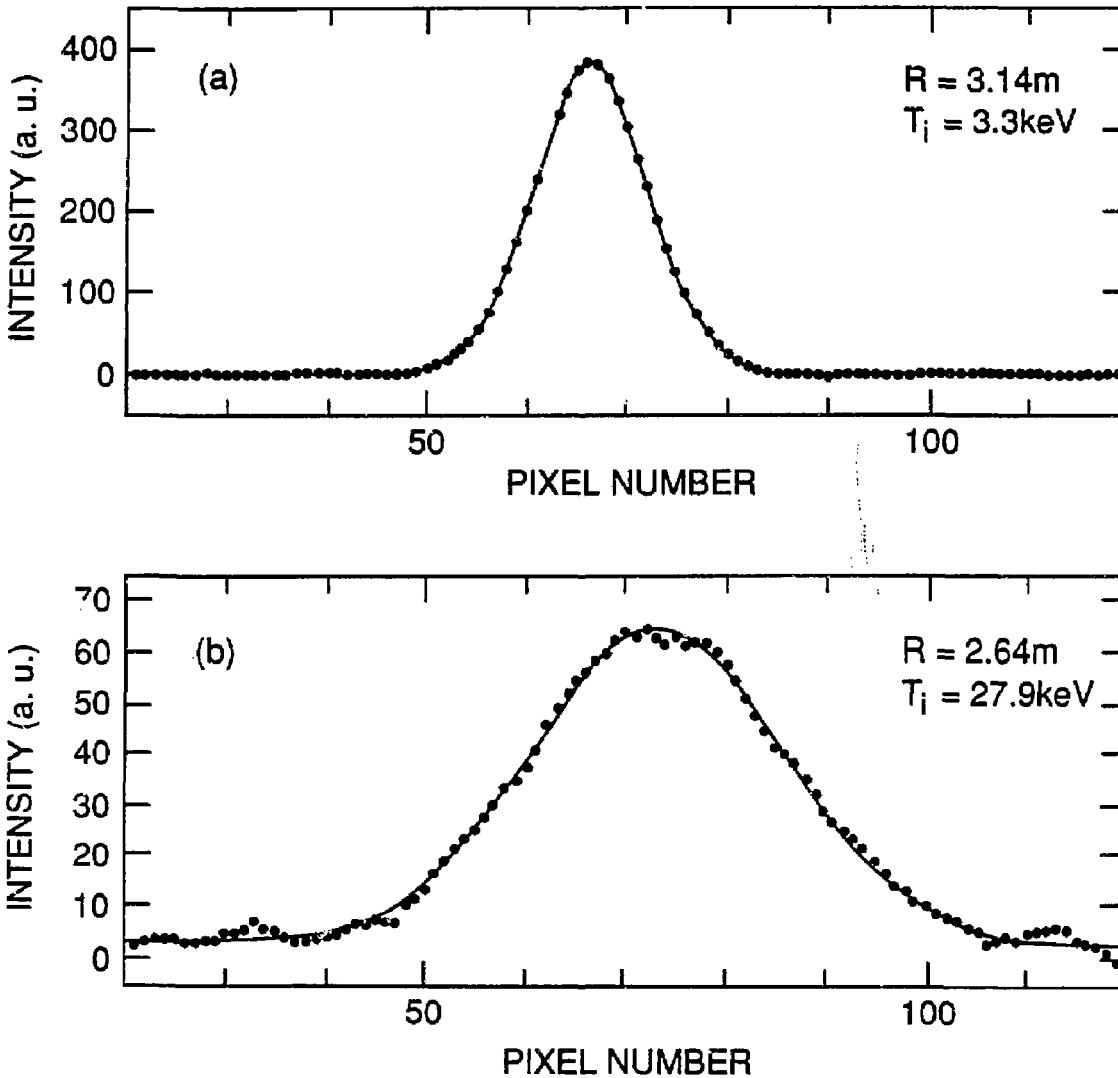
(a)
R = 3.14m
T_i = 3.3keV
INTENSITY (a. u.)
400
300
200
100
0
50
100
PIXEL NUMBER
(b)
R = 2.64m
T_i = 27.9keV
INTENSITY (a. u.)
70
60
50
40
30
20
10
0
50
100
PIXEL NUMBER

Fig. 4

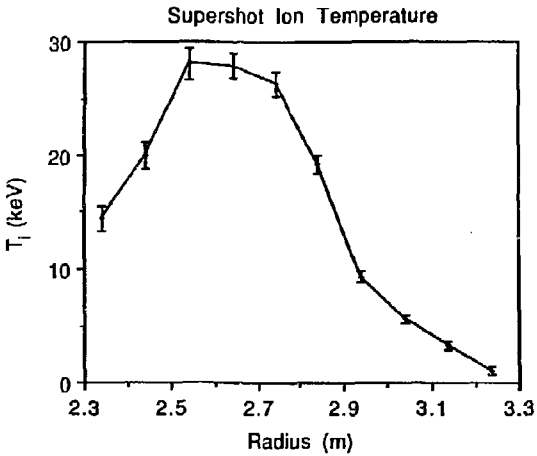
Supershot Ion Temperature
T_i (keV)
30
20
10
0
2.3
2.5
2.7
2.9
3.1
3.3
Radius (m)

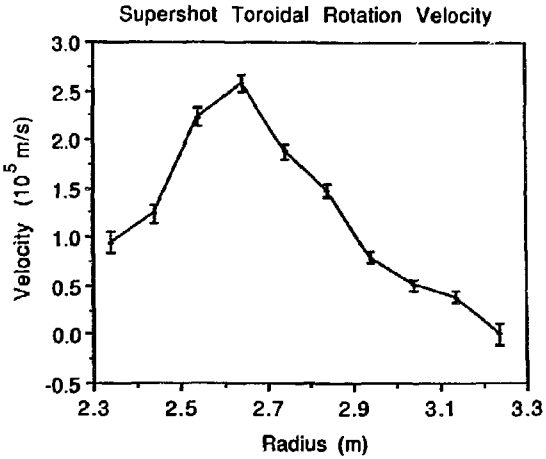
Supershot Toroidal Rotation Velocity
Velocity (10^5 m/s)
3.0
2.5
2.0
1.5
1.0
0.5
0.0
-0.5
2.3
2.5
2.7
2.9
3.1
3.3
Radius (m)

Fig. 5

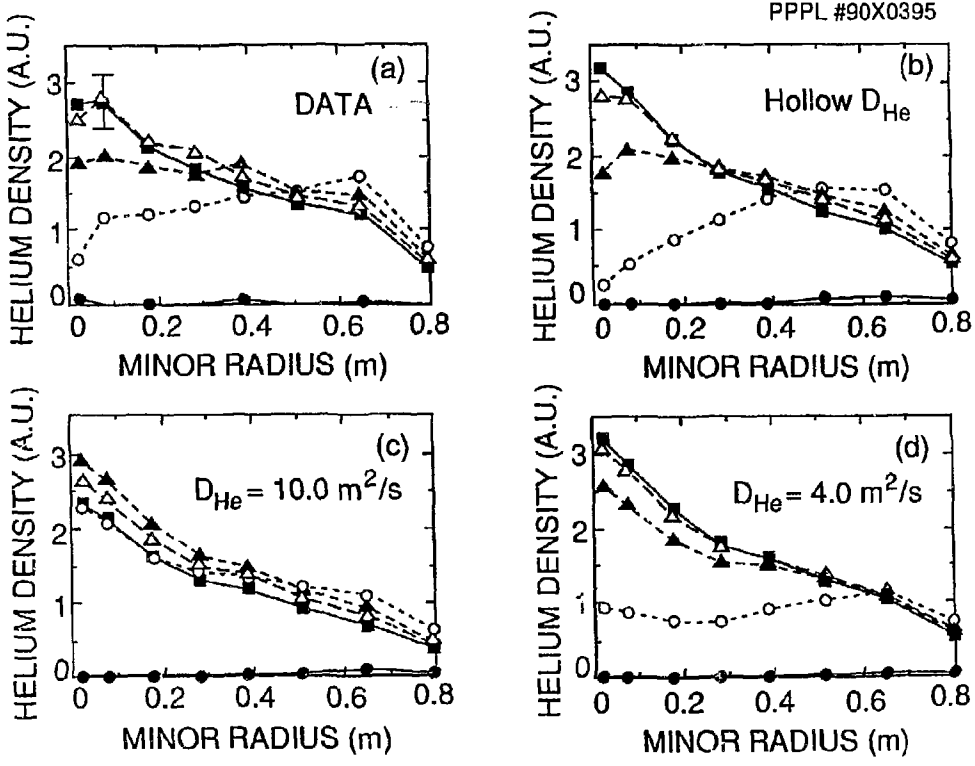
PPPL #90X0395
(a)
DATA
(b)
Hollow D_{He}
(c)
D_{He} = 10.0 m^2/s
(d)
D_{He} = 4.0 m^2/s
HELIUM DENSITY (A.U.)
MINOR RADIUS (m)
0
0.2
0.4
0.6
0.8
1
2
3

Fig. 6

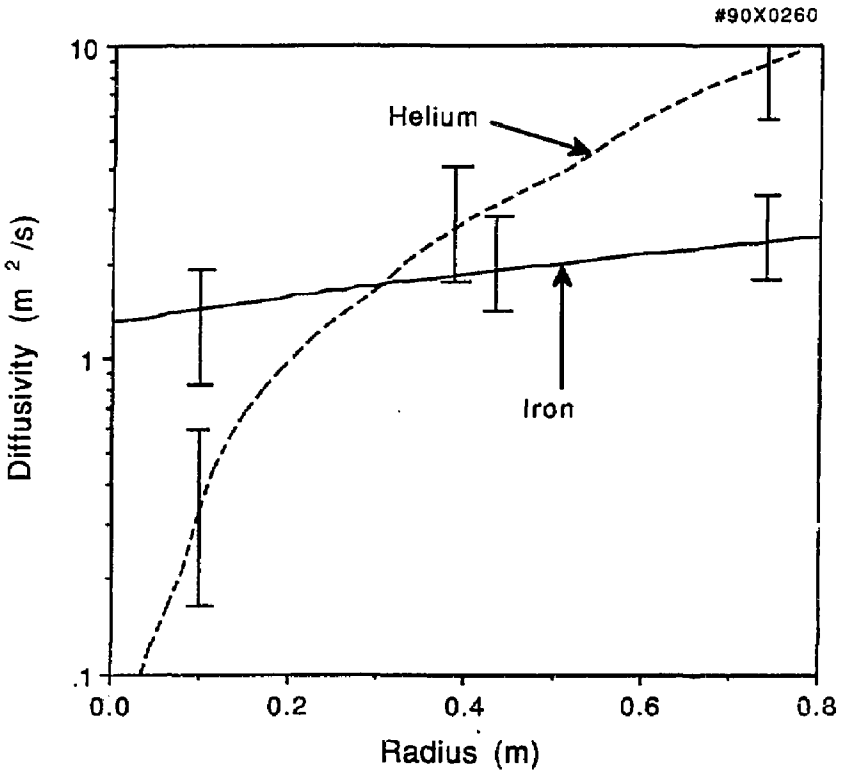
#90X0260
10
1
.1
Diffusivity (m 2 /s)
Helium
Iron
0.0
0.2
0.4
0.6
0.8
Radius (m)

Fig. 7

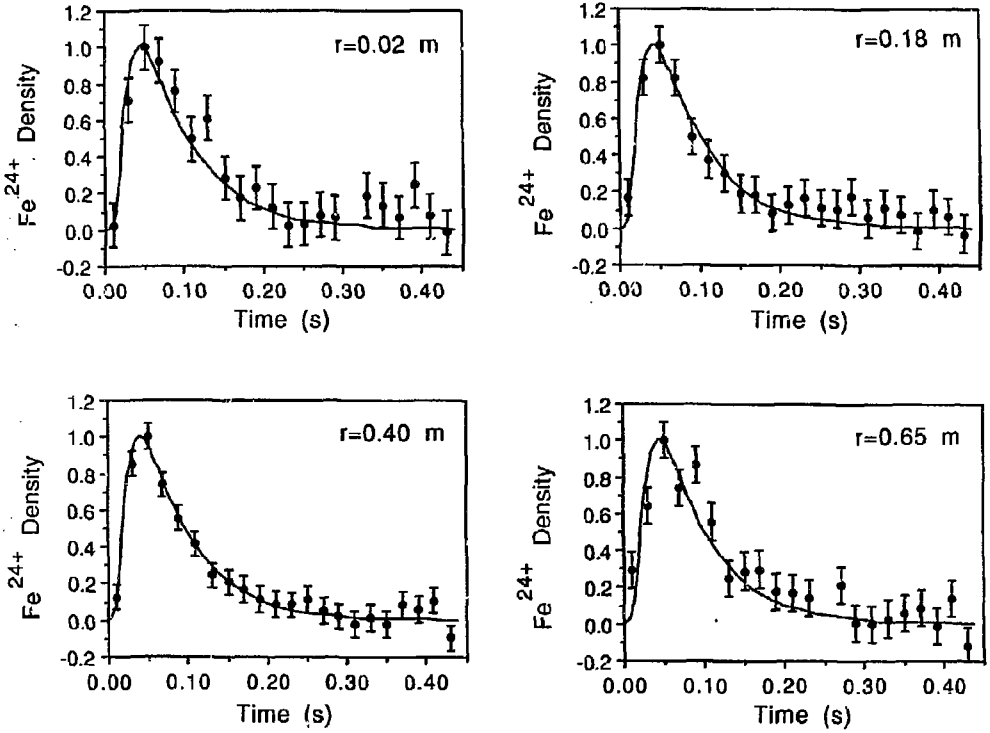
r=0.02 m
r=0.18 m
r=0.40 m
r=0.65 m
Fe24+ Density
Time (s)
1.2
1.0
0.8
0.6
0.4
0.2
0.0
-0.2
0.00
0.10
0.20
0.30
0.40

Fig. 8.